Multilinear Direction Finding for Sensor-Array With Multiple Scales of Invariance

SEBASTIAN MIRON
Université de Lorraine
Vandoeuvre, France

YANG SONG
Universität Paderborn
Paderborn, Germany

DAVID BRIE
Université de Lorraine
Vandoeuvre, France

KAINAM THOMAS WONG
The Hong Kong Polytechnic University
Kowloon, Hong Kong

In this paper, we introduce a novel direction-finding algorithm for a multiscale sensor array, that is, an array presenting multiple scales of spatial invariance. We show that the collected data can be represented as a Candecomp/Parafac model for which we analyze the identifiability properties. A two-stage algorithm for direction-of-arrival estimation with such an array is also proposed. This approach generalizes the results given in [1] to an array that presents an arbitrary number of spatial invariances. We illustrate, on two particular array geometries, that our method outperforms, in some difficult scenarios, the ESPRIT-based approach introduced in [2], the ESPRIT-MUSIC of [3], and the tensor-ESPRIT of [4]. Moreover, we show that the single-snapshot case and the fully cross-correlated sources case can be handled by our method without any spatial smoothing procedure, provided that the array includes at least three scale levels.

Manuscript received August 30, 2013; revised December 1, 2014; released for publication February 9, 2015.

DOI. No. 10.1109/TAES.2015.130576.

Refereeing of this contribution was handled by W. Blanding.

S. Miron and D. Brie were supported by the PHC PROCORE grant 26408PK. Y. Song was supported by The Hong Kong Polytechnic University internal grant G-YL25 and Hong Kong Research Grants Council grant PolyU-5271/12E. K. T. Wong was supported by the France/Hong Kong Joint Research Scheme grant F-HK21/11T and by The Hong Kong Polytechnic University internal grant G-YJ50.

Authors' addresses: S. Miron, D. Brie, Centre de Recherche en Automatique de Nancy (CRAN), UMR 7039, Université de Lorraine, Vandoeuvre, F-54506, France, Email: (sebastian.miron@univ-lorraine.fr, david.brie@univ-lorraine.fr); Y. Song, Universität Paderborn, Department of Electrical Engineering & Information Technology, Paderborn, North Rhine - Westphalia, Germany, Email: (yang.song@connect.polyu.hk); K.T. Wong, Department of Electronic & Information Engineering, The Hong Kong Polytechnic University, Hung Hom, Kowloon, Hong Kong. Corresponding author is S. Miron, Email: (sebastian.miron@univ-lorraine.fr).

I. INTRODUCTION

High-resolution techniques such as multiple signal classification (MUSIC) [5, 6] or estimation of signal parameters via rotational invariance techniques (ESPRIT) [7], introduced in the late 1970s and 1980s, gave an impetus to sensor array signal-processing research. A significant number of eigenstucture-based direction-finding (DF) algorithms have been proposed since for various types of sensors and array configurations. Sidiropoulos et al. [1] proposed for the first time a direction-of-arrival (DOA) estimation approach based on a Candecomp/Parafac (CP) model of the data and highlighted the link between CP and ESPRIT. Over the subsequent years, several other authors proposed CP-based DF algorithms for scalar or vector sensor arrays. Liang et al. [8, 9] proposed two cumulant-based algorithms for source localization using the CP model. DOA-estimation algorithms for vector-sensor-arrays were developed by Guo et al. [10] and by Zhang and Xu [11], based on a three-way CP model, for which an identifiability analysis was provided by Guo et al. [12]. A similar approach, exploiting the quadrilinear structure of the data covariance, was proposed by Miron et al. [13], while Gong [14] developed a trilinear cross-covariance DF method for an array of electric tripoles. Nion and Sidiropoulos [15] established a CP approach for source detection and localization for multi-input multioutput radar systems. A regularized CP-based approach is used by Gong et al. [16] to solve the DOA estimation problem with a single six-component electromagnetic vector sensor. Recently, Zhang et al. [17] proposed an algorithm for coherent angle estimation for bistatic multi-input multioutput radar based on a CP model with linear dependences (i.e., PARALIND). Haardt et al. [4] proposed a higher-order singular value decomposition-based method for multidimensional harmonic retrieval, called tensor-ESPRIT, and showed that it can significantly improve the estimation accuracy compared to the matrix-based methods in some particular situations. Other orthogonal tensor decompositions have also been used in the recent years to construct DF algorithms (see, e.g., [18–20] and the references therein).

The approach proposed in this paper generalizes and extends the tensor-based array-processing approach introduced in [1] to allow an array presenting multiple scales of spatial invariance. Lim and Comon [21] already utilized various tensor decompositions of a small two-dimensional regular array grid with two levels of spatial invariance. They proved that, depending on the coherence of the impinging sources, different decompositions of the array grid are not equivalent, from the performance point of view. However, no generalization to higher dimensions or to arbitrary grid geometry was

provided and no DOA estimation algorithm was proposed. This paper will propose an array geometry for which the incident sources' steering vectors can be expressed as N-way tensor products. As we will show in the subsequent sections, this array configuration may yield a large spatial aperture with a reduced number of elements compared to a fully populated array. In this respect, our method is related to DOA estimation using sparse arrays, a longstanding preoccupation in the sensor array processing community. For example, Sundaram et al. [22] proposed a DOA estimation method for a multielement interferometer with nonuniform spacings, and a computationally efficient technique for the characterization of the resolution and the ambiguity functions of sparse arrays was developed by Goodman and Stiles [23]. For an overview of sparse arrays applications to radar detection, the interested reader is referred to [24] and the references therein. Liao and Chan [25] focused on the problem of DF with a sparse array composed of sensors with unknown gain/phase responses, while Hu et al. [26] highlighted the interest of the recently developed sparse signal reconstruction methods for the DOA estimation with sparse arrays. In our case, the sparse structure of the array results from the multilinear structure sought for the data and the uniqueness conditions for its CP decomposition.

In this paper, we propose a CP-based DF algorithm for any three-dimensional sensor array with an arbitrary number ($\geq$2) of scales of spatial invariance, and we provide a computationally efficient two-stage DOA estimation algorithm that exploits all the information of the sources' DOAs available at each scale level. The DOA estimation is performed using a sequential strategy, progressing from one scale level to the next higher scale level, using an iterative refinement of the direction-cosine estimates within each level. It is worth noting that the concept of multiscale array used in this paper is totally different from that of nested arrays introduced by Pal and Vaidyanathan [27], where the main idea was to use two or more nested uniform linear arrays; the authors of [27] showed that by exploiting the second-order statistics of the received data through the associated difference coarray, more sources than physical sensors can be resolved.

The remainder of this paper is organized as follows. Section II presents the proposed multiscale array configuration. The corresponding data model is derived in Section III. In Section IV, we analyze the identifiability of the proposed data model. A two-stage algorithm for DOA estimation is introduced in Section V. In Section VI, the proposed method is compared in simulations to the ESPRIT-based approach in [2], the ESPRIT-MUSIC algorithm in [3], and the tensor-ESPRIT of [4]. Conclusions are drawn in Section VII.

II. THE GEOMETRIC CONFIGURATION OF A MULTIPLE SCALE-INVARIANT SENSOR ARRAY

We introduce in this section the configuration of the array for which the data model is to be derived in Section III. Consider a subarray composed of L_1 isotropic identical sensors indexed by $l_1 = 1, \ldots, L_1$. Consider then, L_2 identical replicas of this subarray, spatially translated to arbitrary, possibly unknown locations.[1] The L_2 distinct copies of the original subarray, indexed by $l_2 = 1, \ldots, L_2$, can now be seen as subarrays that together constitute a larger (higher level) array. This proposed array structure can be further generalized by considering an additional level, composed of L_3 translated replicas of the previous sensor subarrays, indexed by $l_3 = 1, \ldots, L_3$. Let us generalize this scheme to a total of N such hierarchical levels, with the highest level consisting of L_N subarrays indexed by $l_N = 1, \ldots, L_N$. It is worth noting that two different subarrays at a given level n need not be disjoint, that is, they may have in common subarrays/sensors of the previous level $(n-1)$. However, if all subarrays at each level are disjoint, then the entire array will contain a total number of $L = L_1\, L_2 \ldots L_N$ identical sensors. Fig. 1 illustrates a three-level array of coplanar sensors.

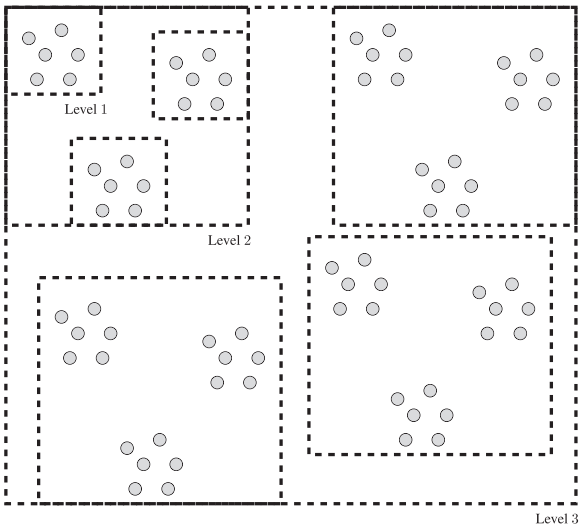

Fig. 1. Multiscale planar array with three hierarchical levels.

Consider also a Cartesian coordinate system $OXYZ$ to describe the considered array. An impinging source is characterized in this coordinate system by its direction-cosines, u, v, w:

$$\begin{bmatrix} u \\ v \\ w \end{bmatrix} = \begin{bmatrix} \sin\theta\cos\phi \\ \sin\theta\sin\phi \\ \cos\theta \end{bmatrix}, \tag{1}$$

where $\theta \in [0, \pi]$ denotes the source's incident elevation angle measured from the positive z axis and $\phi \in [0, 2\pi]$ symbolizes the azimuth angle measured from the positive x axis.

Let us consider a single level-1 subarray. In the coordinate system $OXYZ$, the position of the l_1th sensor

[1] Information on the exact positions of the sensors is not required for the validity of the data model presented in Section III. However, to estimate the sources' DOAs from the measured data, knowledge of the array manifold is necessary.

of this subarray is given by the vector $(x_{l_1}^{(1)}, y_{l_1}^{(1)}, z_{l_1}^{(1)})$. Next, consider L_1 such subarrays. The position of the l_1th sensor of the l_2th subarray is given by $(x_{l_1}^{(1)} + x_{l_2}^{(2)}, y_{l_1}^{(1)} + y_{l_2}^{(2)}, z_{l_1}^{(1)} + z_{l_2}^{(2)})$, where $(x_{l_2}^{(2)}, y_{l_2}^{(2)}, z_{l_2}^{(2)})$ indicates the spatial displacement of the l_2th subarray with respect to the first subarray. It can be easily shown by induction that, for an N-level array, the position of any sensor is given by $(x_{l_1}^{(1)} + \ldots + x_{l_N}^{(N)}, y_{l_1}^{(1)} + \ldots + y_{l_N}^{(N)}, z_{l_1}^{(1)} + \ldots + z_{l_N}^{(N)})$, where $(x_{l_N}^{(N)}, y_{l_N}^{(N)}, z_{l_N}^{(N)})$ indicates the spatial displacement of the l_Nth subarray compared to the first subarray of the level N (indexed by $l_N = 1$), etc.

The above presented array structure is composed of sensors/subarrays packs that differ from each other only by a translation in the three-dimensional Euclidian space. This provides interesting spatial invariance properties in the data acquired by this array, as will be shown in the next section.

III. DATA MODEL

A. Derivation of the CP Model

Consider first a narrow-band plane wave impinging on the array described in Section II. Let us represent by $a_{l_1 l_2 \ldots l_N}$ its phase factor at the sensor indexed by $l_1, l_2, \ldots, l_N$ at the N various levels of the array. Define $\mathbf{k} = [u\ v\ w]^T$ and $\mathbf{d}_{l_n}^{(n)} = [x_{l_n}^{(n)}\ y_{l_n}^{(n)}\ z_{l_n}^{(n)}]^T$, with $n = 1, \ldots, N$. With the notation introduced above, the spatial phase factor is given by:

$$a_{l_1 l_2 \ldots l_N}(\mathbf{k}) = \exp\left\{ j \frac{2\pi}{\lambda} \sum_{n=1}^{N} \mathbf{k}^T \mathbf{d}_{l_n}^{(n)} \right\} = \prod_{n=1}^{N} \exp\left\{ j \frac{2\pi}{\lambda} \mathbf{k}^T \mathbf{d}_{l_n}^{(n)} \right\}. \quad (2)$$

Thus, the array manifold for the entire sensor array is

$$\mathbf{a}(\mathbf{k}) = \mathbf{a}_1(\mathbf{k}) \otimes \ldots \otimes \mathbf{a}_N(\mathbf{k}), \quad (3)$$

with

$$\mathbf{a}_n(\mathbf{k}) = \begin{bmatrix} e^{j\left(2\pi/\lambda\right)\mathbf{k}^T \mathbf{d}_1^{(n)}} \\ \vdots \\ e^{j\left(2\pi/\lambda\right)\mathbf{k}^T \mathbf{d}_{L_n}^{(n)}} \end{bmatrix} \quad (4)$$

an $L_n \times 1$ vector, $\forall n = 1, \ldots, N$ and $\otimes$ represents the Kronecker product of two matrices.

Next, consider P narrow-band plane waves, having traveled through a nonconductive homogeneous isotropic medium, impinging upon the array from directions $\mathbf{k}_p = [u_p\ v_p\ w_p]^T$, with $p = 1, \ldots, P$. Denote by $s_p(t)$ the time signal emitted by the pth narrow-band source.[2] Then, the output at time t of the entire sensor array can be expressed as an $L \times 1$ vector,

$$\mathbf{z}(t) = \sum_{p=1}^{P} \left(\mathbf{a}_1\left(\mathbf{k}_p\right) \otimes \ldots \otimes \mathbf{a}_N\left(\mathbf{k}_p\right)\right) s_p(t) + \mathbf{n}(t), \quad (5)$$

where $\mathbf{n}(t)$ is a complex-valued zero-mean additive white noise.

Let us assume that we have at our disposal K snapshots at time instants, $t_1, t_2, \ldots, t_K$. Define the following $L_n \times P$ matrices:

$$\mathbf{A}_1 = [\mathbf{a}_1(\mathbf{k}_1), \ldots, \mathbf{a}_1(\mathbf{k}_P)] \quad (6)$$

$$\vdots$$

$$\mathbf{A}_N = [\mathbf{a}_N(\mathbf{k}_1), \ldots, \mathbf{a}_N(\mathbf{k}_P)], \quad (7)$$

and the $K \times P$ matrix:

$$\mathbf{S} = \begin{bmatrix} s_1(t_1) & s_2(t_1) & \ldots & s_P(t_1) \\ s_1(t_2) & s_2(t_2) & \ldots & s_P(t_2) \\ \vdots & \vdots & \ddots & \vdots \\ s_1(t_K) & s_2(t_K) & \ldots & s_P(t_K) \end{bmatrix} = [\mathbf{s}_1, \mathbf{s}_2, \ldots, \mathbf{s}_P]. \quad (8)$$

The collection of K snapshots of the array can then be organized into an $L \times K$ data matrix as

$$\mathbf{Z} = [\mathbf{z}(t_1), \ldots, \mathbf{z}(t_K)] = (\mathbf{A}_1 \odot \ldots \odot \mathbf{A}_N)\mathbf{S}^T + \mathbf{N}, \quad (9)$$

where $\odot$ denotes the Khatri-Rao (Kronecker columnwise) product of two matrices, and $\mathbf{N}$ is a $(L \times K)$ complex-valued matrix, modeling the noise on the entire array for all K temporal snapshots. Equation (9) reveals a $(N+1)$-dimensional CP structure (see [28, 29]) of the collected data.

In the case where only one time-sample is available, that is, matrix $\mathbf{S}$ is a $1 \times P$ vector, the data model given by (9) becomes

$$\mathbf{z} = (\mathbf{A}_1 \odot \ldots \odot \mathbf{A}_N)\mathbf{s} + \mathbf{n}, \quad (10)$$

with $\mathbf{z} = \mathbf{z}(t_1)$, $\mathbf{s} = \mathbf{s}(t_1) = (\mathbf{S}(1, :))^T$ and $\mathbf{n} = \mathbf{N}(:, 1)$. In the definitions above, we used the Matlab notations for columns and rows selection operators. Equation (10) is a vectorized representation of a N-dimensional CP data model (see, e.g., [30] for details on the different CP representations). It is worth noting that if only one snapshot of the array is available, the $N+1$ CP model degenerates into an N-dimensional one.

B. CP Versus ESPRIT

We will next briefly contrast CP with ESPRIT for the proposed array configuration. For fuller information on this topic, the reader is referred to [1, 31] and the references therein. Consider a two-level array composed of L_2 subarrays, each of L_1 sensors. Denote by $\mathbf{B}_{l_2}$, with $l_2 = 1, \ldots, L_2$, the $L_1 \times P$ steering vector matrices for the L_2 subarrays. With the notation introduced above, it can be easily seen that $\mathbf{B}_1 = \mathbf{A}_1$, and $\mathbf{B}_{l_2} = \mathbf{B}_1 \mathbf{\Phi}_{l_2}$,

[2] The incident signals are narrowband in that their bandwidths are very small compared with the inverse of the wavefronts' transit time across the array.

$(l_2 = 2, \ldots, L_2)$, where

$$\mathbf{\Phi}_{l_2} = \text{diag}\left(e^{j\left(2\pi/\lambda\right)\mathbf{k}_1^T\mathbf{d}_{l_2}^{(2)}}, \ldots, e^{j\left(2\pi/\lambda\right)\mathbf{k}_P^T\mathbf{d}_{l_2}^{(2)}}\right). \quad (11)$$

In (11), diag(.) denotes a square diagonal matrix with the elements in the argument on its main diagonal. The data measured on the L_2 subarrays can be represented by a set of $(L_1 \times K)$ matrices $\mathbf{Z}_{l_2}$, $(l_2 = 1, \ldots, L_2)$

$$\mathbf{Z}_{l_2} = \mathbf{B}_{l_2}\mathbf{S}^T + \mathbf{N}_{l_2} = \mathbf{A}_1\mathbf{\Phi}_{l_2}\mathbf{S}^T + \mathbf{N}_{l_2}, \quad (12)$$

where $\mathbf{N}_{l_2}$ represents the additive noise on the l_2th subarray. With this new notation, the CP model (9) for the considered two-level array becomes:

$$\begin{aligned}\mathbf{Z} &= \begin{bmatrix}\mathbf{Z}_1\\ \mathbf{Z}_2\\ \vdots\\ \mathbf{Z}_{L_2}\end{bmatrix} = \begin{bmatrix}\mathbf{A}_1\\ \mathbf{A}_1\mathbf{\Phi}_2\\ \vdots\\ \mathbf{A}_1\mathbf{\Phi}_{L_2}\end{bmatrix}\mathbf{S}^T + \begin{bmatrix}\mathbf{N}_1\\ \mathbf{N}_2\\ \vdots\\ \mathbf{N}_{L_2}\end{bmatrix}\\ &= (\mathbf{A}_1 \odot \mathbf{A}_2)\,\mathbf{S}^T + \mathbf{N}. \quad (13)\end{aligned}$$

The standard ESPRIT algorithm [32] exploits the invariance structure of the signal subspace for a single pair of data matrices $\{\mathbf{Z}_{l_2}, \mathbf{Z}_{l_{2'}}\}$ and estimates the corresponding matrix $\mathbf{\Phi}$ that links these two matrices' respective signal subspace. CP makes use of the entire dataset $\{\mathbf{Z}_{l_2}, \forall l_2 = 1, \ldots, L_2\}$ simultaneously, thus exploiting simultaneously the displacement invariance relationships between all the subarrays, by using a multilinear model of the data and the matrix $\mathbf{A}_2$. A multiple invariance ESPRIT approach, using all available invariance, has also been proposed in [32], leading to a nonlinear, computationally complex optimization problem. More recently, a tensor-ESPRIT approach was proposed in [4] for multidimensional harmonic retrieval; however, unlike the CP-based approach proposed in this paper, this method requires a very particular array structure, presenting shift invariances within each scale level.

IV. DATA MODEL IDENTIFIABILITY

Before presenting the proposed algorithm for DOA estimation, a discussion on data model identifiability is in order. In this paper, the term identifiability refers to the nonambiguous estimation of the parameters of the CP model from the collected data. We will focus on the identifiability conditions for the estimation of the matrices $\mathbf{A}_1, \ldots, \mathbf{A}_N$ and $\mathbf{S}$, from the data (9). A brief discussion on the ambiguity problems when estimating the direction-cosines from $\mathbf{A}_1, \ldots, \mathbf{A}_N$ is provided in Section V.

The main advantage of the CP method, compared to other source separation approaches, is CP model identifiability under only mild conditions. Kruskal [33] derived a sufficient condition for identifiability in the three-way CP model. This condition is based on a special notion of matrix rank, called the Kruskal-rank or k-rank. The k-rank of a matrix is the maximum number of linearly independent columns that can be selected from that matrix in an arbitrary manner. Thus, the k-rank of a matrix is at most equal to its classical rank. Kruskal's identifiability condition has been generalized later to N-way arrays by Sidiropoulos and Bro [34]. If applied to the data model given by (9), this condition states that the matrices $\mathbf{A}_1, \ldots, \mathbf{A}_N$ and $\mathbf{S}$ can be almost uniquely estimated from $\mathbf{Z}$ if

$$\sum_{n=1}^{N} k_{\mathbf{A}_n} + k_{\mathbf{S}} \geq 2P + N, \quad (14)$$

where $k_{(.)}$ denotes the k-rank of a matrix. This estimation is unique up to two trivial indeterminacies. The first indeterminacy is an arbitrary simultaneous column permutation of all $N + 1$ matrices and implies that an a priori defined order of the sources cannot be posteriori determined. The second one is an arbitrary column scaling/counterscaling and can be resolved by normalizing each column of matrices $\mathbf{A}_1, \ldots, \mathbf{A}_N$ by that column's first element.

If the P sources have distinct DOAs and are not fully cross-correlated, the identifiability condition (14) can be reformulated as

$$\sum_{n=1}^{N} \min(L_n, P) + \min(K, P) \geq 2P + N. \quad (15)$$

In general, the number of snapshots exceeds the number of sources (i.e., $K > P$), in which case (15) becomes

$$\sum_{n=1}^{N} \min(L_n, P) \geq P + N. \quad (16)$$

Furthermore, if $L_n > P, \ \forall n = 1, \ldots, N$ (this could be the case especially for a small N), the sufficient condition will always be met if $P, N \geq 2$. This means that, for sources that are noncollocated and also not fully cross-correlated, the CP model identifiability can be realized in most practical applications.

Another case of interest is when the array has at least three scales of invariance. In this situation, the model can be identified even with only a single snapshot, and Kruskal's condition reads:

$$\sum_{n=1}^{N} \min(L_n, P) \geq 2P + N - 1. \quad (17)$$

Meanwhile, if condition (14) does not hold, the identifiability of (9) can no longer be ensured. In this case, partial identifiability may apply, meaning that only some of the parameters in (9) may be uniquely recovered. This partial-identifiability Kruskal-like condition, for the three-way CP model, has been derived in [35]. A generalization of these results to N-way arrays has been proposed in [36]. Specific identifiability conditions for the case of fully coherent sources and/or collocated sources could be derived from these results. However, this analysis would be beyond the scope of this paper.

V. DOA ESTIMATION

The DOA estimation procedure proposed in this paper can be split into two stages. The first stage estimates the N steering vectors $\mathbf{a}_n(\mathbf{k}_p)$ ($n = 1, \ldots, N$) for each of the P sources ($p = 1, \ldots, P$), by exploiting the CP structure (9) of the collected data. In this first stage, an alternating least-squares (ALS) procedure can be used to fit the CP model. This ALS procedure recursively estimates one of the $N + 1$ matrices $\mathbf{A}_1, \ldots, \mathbf{A}_N, \mathbf{S}$, by fixing the other N of them [28, 29]. The algorithmic steps of ALS can be simply stated, but the algorithm suffers from slow convergence and is sensitive to over- (and under-) estimation of the number of sources. Improved versions of ALS, using data compression and line search techniques that partly mitigate these deficiencies, have been proposed in [37–39]. Derivative-based methods or direct (noniterative) procedures can likewise be employed to fit the CP model [40]. Such CP decomposition methods have been implemented in Matlab and are freely available online (see, e.g., [41, 42]). This present paper's simulations will use the COMFAC approach of [38] because of its algorithmic efficiency.

The second stage estimates the source's direction-cosines $\mathbf{k}_p$, $p = 1, \ldots, P$ from the steering vectors obtained at the previous stage. To this end, we propose to formulate the DOA estimation as an optimization problem and to adopt a new sequential procedure that exploits all the available information from the source's steering vectors encompassing all scale levels.

Define the following cost functions:

$$\mathcal{J}_n\left(\mathbf{k}_p\right) = \left\|\hat{\mathbf{a}}_n^p - \mathbf{a}_n\left(\mathbf{k}_p\right)\right\|^2, \text{ with } n = 1, \ldots, N, \quad (18)$$

where $\hat{\mathbf{a}}_n^p$ denotes the estimated steering vector at the nth level for the pth source. Estimating the DOAs for the pth source comes down to minimizing the following criterion:

$$\mathcal{I}_N\left(\mathbf{k}_p\right) = \sum_{n=1}^{N} \mathcal{J}_n\left(\mathbf{k}_p\right). \quad (19)$$

This function is nonconvex and highly nonlinear with respect to the direction-cosines; hence, a direct local optimization procedure would fail in most cases. We propose to adopt a new sequential strategy to minimize $\mathcal{I}_N(\mathbf{k}_p)$, progressing from one level to the next higher level, using an iterative refinement of the direction-cosine estimates within each level. The method is based on the fact that, when noise-free, the N cost functions in (18) have the same global minimum.

Assume that the level-1 subarrays' intersensor separations do not exceed half a wavelength. This assumption is essential to obtaining a set of high-variance but unambiguous direction-cosine estimates. On the contrary, to achieve a practical advantage, it is important that the spatial displacement between any two subarrays of the highest level exceeds $\lambda/2$, where λ is the wavelength. This will produce estimates of lower variance but with cyclic ambiguity for the same set of direction-cosines. On the other hand, under the first assumption, the $\mathcal{J}_1(\mathbf{k}_p)$ function is unimodal on the support region of the DOAs. Therefore, any local optimization procedure should converge toward the global minimum for the criterion. Thus, we obtain another set of estimates, now of high variance but with no cyclic ambiguity, for the DOAs, to be denoted by $\mathbf{k}_{p,1}^*$ with $p = 1, \ldots, P$. These estimates will subsequently be used, in a second step, as the initial point for the minimization of

$$\mathcal{I}_2\left(\mathbf{k}_p\right) = \mathcal{J}_1\left(\mathbf{k}_p\right) + \mathcal{J}_2\left(\mathbf{k}_p\right). \quad (20)$$

Because no assumption is made on the distances between the level-2 subarrays, $\mathcal{I}_2(\mathbf{k}_p)$ may present more than one local minimum. Hence, a good initial estimate is crucial for the optimization procedure. The estimates obtained by the minimization of $\mathcal{I}_2(\mathbf{k}_p)$, denoted by $\mathbf{k}_{p,2}^*$, are then used for the minimization of $\mathcal{I}_3(\mathbf{k}_p) = \sum_{n=1}^{3} \mathcal{J}_n(\mathbf{k}_p)$, and so on, until the final estimates are obtained by the minimization of $\mathcal{I}_N(\mathbf{k}_p)$.

We emphasize the necessity of sequential iteration for good results, going from level n to level $n + 1$. A direct jump from a low hierarchical level (e.g., level 1) to a high hierarchical level (e.g., level N) may result in erroneous results, especially for low signal-to-noise ratios (SNRs). The reason is that the number of local minima for $\mathcal{J}_n(\mathbf{k})$ and $\mathcal{I}_n(\mathbf{k})$ increases with n and that the low-level estimates have a high variance. Thus, the direct initialization of a high-level parameter estimation step with a low-level estimate may result in misconvergence toward a local minimum instead of the global one.

This sequential minimization can be regarded as a graduated nonconvexity (GNC) optimization approach [43] because the criterion to minimize is gradually transformed from $\mathcal{I}_1$ to $\mathcal{I}_N$; the main difference from GNC is that, in our approach, the criterion transformation is determined a priori, by the intersensor/subarray spacings, while in GNC, this transformation is user defined. A sufficient condition ensuring the global minimization of the nonconvex problem is that the initial convex problem has a global minimum that can be reached and that each intermediate subproblem has a global minimum lying in a locally convex region that surrounds the next level's global minimum. The first requirement is met because the interelement spacing of the level-1 subarray is $\leq \lambda/2$, resulting in a unimodal criterion $\mathcal{J}_1(\mathbf{k})$. Regarding the second requirement, it is difficult to determine whether it is met because the shape of the criterion $\mathcal{J}_N(\mathbf{k})$ depends on the array geometry. However, as the number of local minima increases with the intersensor spacings, the algorithm would likely reach the global minimum of the criterion $\mathcal{J}_N(\mathbf{k})$, provided that the intersensor spacings of the successive levels of the array do not change excessively from one level to another level.

The proposed two-stage estimation algorithm can be summarized as follows:

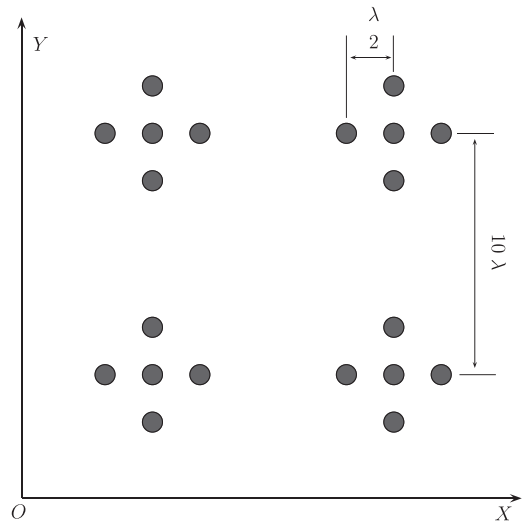

Fig. 2. Spatial configuration of sensor array used in simulations of sub-Section VIA.

FIRST STAGE: Estimate $\mathbf{A}_1, \ldots, \mathbf{A}_N$ by CP decomposition of the data $\mathbf{Z}$ or $\mathbf{z}$, that is, see (9) or (10).

SECOND STAGE:

- For $p = 1, \ldots, P$ and for $n = 1, \ldots, N$, compute

$$\mathbf{k}_{p,n}^{*} = \underset{\mathbf{k}_p}{\operatorname{argmin}}\ \mathcal{I}_n\left(\mathbf{k}_p\right) = \underset{\mathbf{k}_p}{\operatorname{argmin}} \sum_{i=1}^{n} \mathcal{J}_i\left(\mathbf{k}_p\right). \quad (21)$$

- *Output:* the estimated parameters for the P sources: $\hat{\mathbf{k}}_p = (\hat{u}_p, \hat{v}_p, \hat{w}_p) = \mathbf{k}_{p,N}^{*}$ with $p = 1, \ldots, P$.

The next section will illustrate the performance of the proposed algorithm via Monte-Carlo simulations.

VI. SIMULATION RESULTS AND DISCUSSION

First, we compare our approach with the two ESPRIT-based methods developed in [2, 3]. In the second part of this section, a comparison with another tensor-based algorithm for harmonic estimation, that is, tensor-ESPRIT of [4], is conducted.

A. Comparison With the ESPRIT-Based Approaches of [2] and [3]

In this subsection, we compare our approach with the dual-sized ESPRIT of [2] and the ESPRIT with MUSIC-based disambiguation introduced in [3], using an array configuration proposed by those same authors. The Cramér-Rao bound (CRB) for the considered model, derived in the Appendix, is used as a benchmark. The sensor-array consists of a 2×2 square grid at an extended spacing of 10λ and a five-element half-wavelength spaced cross-shaped subarray at each grid point, as illustrated by Fig. 2. We adopt this particular array configuration because it is one of the configurations proposed in [2] and [3] to which our approach is compared. Nevertheless, the method proposed in this paper is much more general and does not require a regular grid or a regular shape subarray, as shown in Section II. This array can be seen as having two hierarchical levels with $L_1 = 5$ sensors and $L_2 = 4$ subarrays, or as a three-level array with $L_1 = 5$, $L_2 = 2$, and $L_3 = 2$. In [2], the sources' DOAs are estimated using an ESPRIT-based technique. Two types of estimates (coarse-but-unambiguous vs. fine-but-cyclically-ambiguous) are computed separately (and in parallel) for each of the x and y axes of the considered spatial grid, using four matrix pencils altogether. The coarse-but-unambiguous estimates are then used to disambiguate the fine-but-cyclically-ambiguous DOA estimates. This procedure is followed by a pairing step of the x-axis and y-axis direction-cosines of the sources. In [3], the fine-but-cyclically-ambiguous DOA estimates obtained by ESPRIT are disambiguated using a MUSIC-like algorithm. The main advantage of this approach over [2] is that there is no need for an explicit derivation of any coarse reference estimate. Moreover, the algorithm benefits from the superior accuracy of MUSIC while avoiding its computational burden.

For the results presented in this subsection, the first stage of the proposed algorithm is performed using the COMFAC CP-fitting algorithm for complex valued three-way arrays, available at http://www.telecom.tuc.gr/∼nikos/. For the second stage, the minimization of $\mathcal{I}_n$ in (21) is done by the Nelder-Mead simplex algorithm, initialized by the estimates of the previous step $\mathbf{k}_{p,n-1}^{*}$. Random values, within the parameters' respective support regions, are used to initialize the minimization of $\mathcal{I}_1 = \mathcal{J}_1$.

The considered signal scenario involves two equal-power narrowband signals impinging respectively from $(u_1 = 0.83, v_1 = 0.17)$ and $(u_2 = 0.13, v_2 = 0.79)$. There are $I = 500$ independent Monte-Carlo runs for each data point plotted on the figures. The additive white noise is complex-value Gaussian distributed. All the figures plot the composite root-mean-square-error (CRMSE) of the sources' Cartesian direction-cosine estimates versus SNR. This CRMSE is defined as

$$\frac{1}{I}\sum_{i=1}^{I}\sqrt{\frac{\delta_{u,p,i}^2 + \delta_{v,p,i}^2}{2}}, \quad (22)$$

where $\delta_{u,p,i}(\delta_{v,p,i})$ symbolizes the error in estimating the pth source's x-axis (y-axis) direction-cosine during the ith run.

The pth source's signal model used for the simulations represented on Figs. 3–6 is

$$s_p(t) = a_p(t)\, e^{j\left(2\pi \frac{f_p}{3} t + \varphi_p\right)}, \quad (23)$$

where $a_p(t)$ is a zero-mean unit-variance complex-value time series, Gaussian distributed, and temporally white; φ_p is a random variable uniformly distributed between $[0, 2\pi]$; and $f_1 = f_2 = 1$. In Figs. 3–5, the two complex signals—$a_1(t)$ and $a_2(t)$—are statistically independent. All random entities are statistically independent of each other.

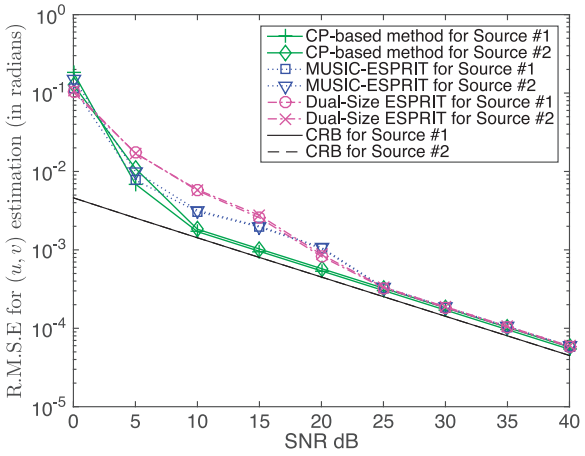

(a) $K = 5$

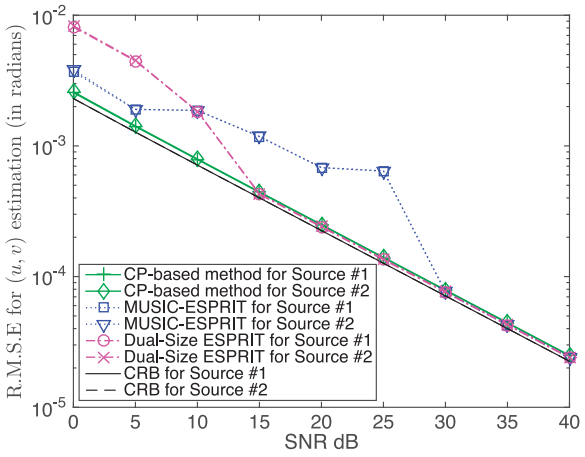

(b) $K = 20$

Fig. 3. Statistically independent sources: CRMSE versus signal-to-noise power ratio (SNR).

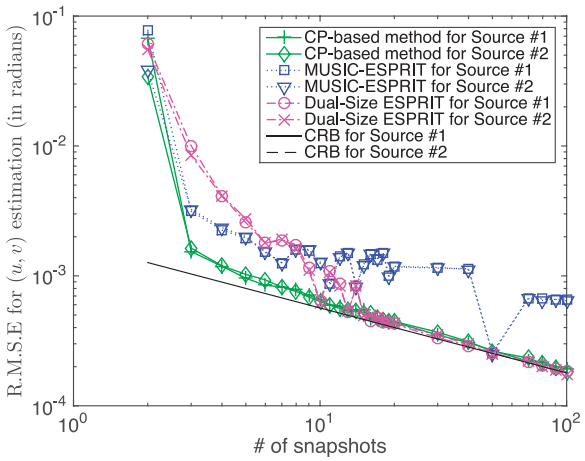

Fig. 4. Statistically independent sources: CRMSE versus number of snapshots when SNR = 15 dB.

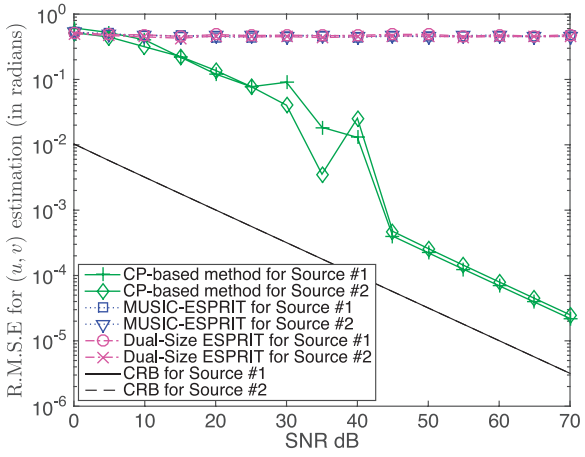

Fig. 5. Statistically independent sources: CRMSE versus signal-to-noise power ratio (SNR) using one temporal snapshot.

The first experiment evaluates the performance of the three algorithms for different SNRs in the case of statistically independent sources. Figs. 3a and 3b plot the CRMSE for $K = 5$ and $K = 20$ snapshots, respectively. For high SNRs, the two approaches yield similar results, very close to the CRBs. However, at low SNRs, the proposed algorithm outperforms the ESPRIT-based algorithms. This advantage is more obvious at small values of K. The explanation is that our method estimates also the incident signals' temporal waveforms. This is not the case for the methods in [2, 3], which average over the time dimension to estimate the data spatial covariance matrix. Thus, CP estimates only $(L_1 + L_2 + K)P$ number of parameters, but $L_1\ L_2\ P$ for ESPRIT. Roughly speaking, our algorithm provides better results compared to the other methods for small values of K. Fig. 4 further illustrates this statement using different numbers of snapshots $K = \{2, 3, \ldots, 19, 20, 30, 40, \ldots, 90, 100\}$ for an SNR of 15 dB. It can be observed that the multiscale CP approach produces more accurate results for a number of snapshots fewer than about $K = 11$, which agrees with the simplified analysis above.

The second experiment demonstrates the applicability of the proposed algorithm for a single snapshot. However, the $(N + 1)$-way CP model now degenerates into an N-way one, as shown by (10). Therefore, the array depicted on Fig. 2 is now seen as a three-level array, where the first level is the five-element cross-shaped subarray ($L_1 = 5$), the second level is composed of two such subarrays, aligned along the x-axis ($L_2 = 2$), and the third level consists of two level-2 subarrays ($L_3 = 2$). Fig. 5 plots the results for the three methods under the single-snapshot scenario. It can be seen that the proposed method still yields fair results, while ESPRIT and ESPRIT-MUSIC are unusable here.

In a third experiment, we study the behavior of the three approaches for cross-correlated sources. For that, we simulated two sources with a cross-correlation coefficient of 0.83 between $a_1(t)$ and $a_2(t)$. The numerical simulation results are plotted in Fig. 6. Once again, the proposed algorithm outperforms the ESPRIT-based methods. This is because, in this case, the source covariance matrix is no longer diagonal, which violates a restriction in the model used in [2] and [3], while entirely allowed by our CP

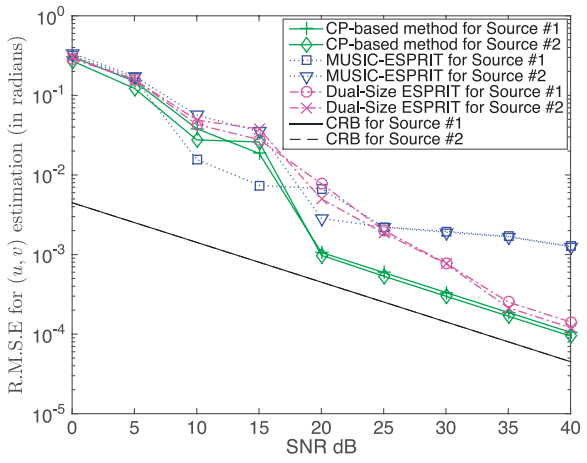

(a) $K = 5$

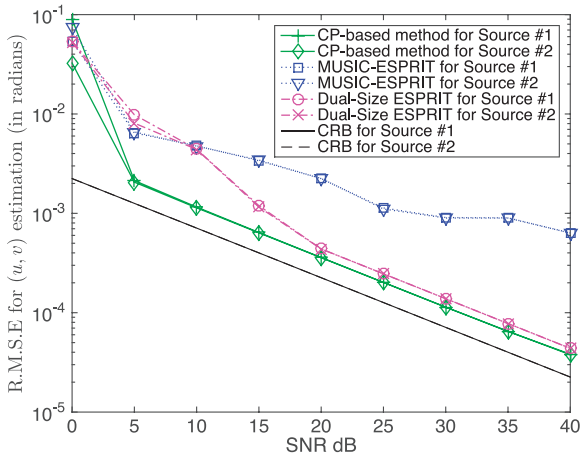

(b) $K = 20$

Fig. 6. Cross-correlated sources: CRMSE versus signal-to-noise power ratio (SNR).

approach. However, a strong cross-correlation between sources may cause problems for our algorithm with convergence, especially for a low SNR and a small number of snapshots, as one can see in Fig. 6a. Anyway, in this case, the ESPRIT-MUSIC also gives inaccurate results even for high SNRs. This is because the cross-correlation causes, for the MUSIC disambiguation procedure of [3], inaccurate estimation of the signal subspace and the noise subspace.

B. Comparison With the Tensor-ESPRIT Approach of [4]

In this subsection, our approach is compared to the R-dimensional (R-D) standard tensor-ESPRIT and the R-D unitary tensor-ESPRIT developed in [4]. The main difference between the two tensor-ESPRIT algorithms is that R-D unitary tensor-ESPRIT uses a forward-backward averaging preprocessing step that virtually doubles the number of available snapshots without sacrificing the array aperture.

In order to apply R-D tensor-ESPRIT-type methods, the sensor array must feature shift invariances in each of

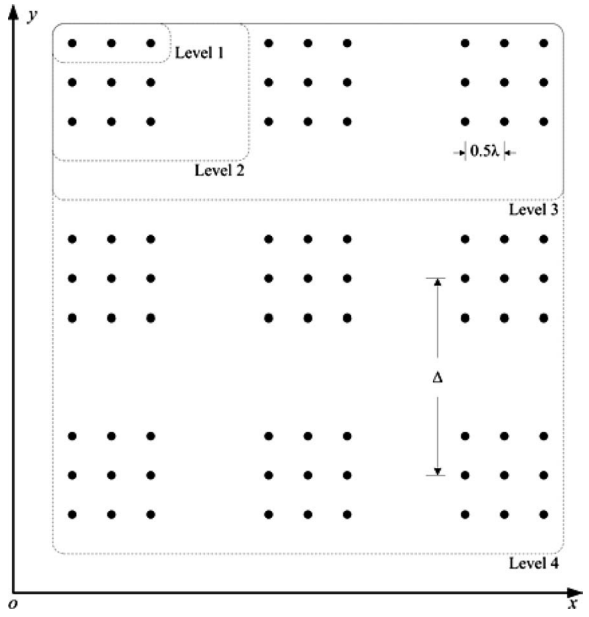

Fig. 7. Spatial configuration of sensor array used in simulations of sub-Section VIB.

its modes; let us mention once again that this geometrical constraint is not required by our CP-based method. For the numerical experiments presented in this subsection, the simulated array consists of a 3×3 uniform square grid at an extended spacing of Δ and a 3×3 half-wavelength spaced uniform square subarray at each grid point, as illustrated by Fig. 7. In all simulations, except for the ones presented on Fig. 10, the value of Δ is set to 10λ.

For the proposed approach, this array can be seen as having four hierarchical levels with $L_1 = L_2 = L_3 = L_4 = 3$, and the steering vectors of the pth signal for each level are

$$\mathbf{a}_1(u_p) = \left[1,\ e^{j\pi u_p},\ e^{j\pi 2u_p}\right]^T,$$
$$\mathbf{a}_2(v_p) = \left[1,\ e^{j\pi v_p},\ e^{j\pi 2v_p}\right]^T,$$
$$\mathbf{a}_3(u_p) = \left[1,\ e^{j\frac{2\pi\Delta}{\lambda}u_p},\ e^{j\frac{2\pi\Delta}{\lambda}2u_p}\right]^T,$$
$$\mathbf{a}_4(v_p) = \left[1,\ e^{j\frac{2\pi\Delta}{\lambda}v_p},\ e^{j\frac{2\pi\Delta}{\lambda}2v_p}\right]^T.$$

It is worth noting that the direction-cosines u_p, $p = 1, \ldots P$ are only involved in the level-1 and level-3 subarrays, while direction-cosines v_p, $p = 1, \ldots P$ are involved in only the level-2 and level-4 subarrays. Thus, the four-level minimization problem can be decoupled into two independent two-level minimization problems.

For R-D tensor-ESPRIT, a total number of $3^4 = 81$ sensors, are distributed among $N = 4$ dimensions $(3 \times 3 \times 3 \times 3)$ with uniform spacing in all modes. The tensor-based signal subspace $\mathcal{U}^{[s]}$, defined in (21) of [4], is firstly found by any higher-order singular value decomposition-based low-rank approximation of the

measurement tensor $\mathcal{Y} \in \mathbb{C}^{3\times3\times3\times3\times K}$:

$$\mathcal{Y} = \sum_{p=1}^{P} \mathbf{a}_1\left(u_p\right) \circ \mathbf{a}_2\left(v_p\right) \circ \mathbf{a}_3\left(u_p\right) \circ \mathbf{a}_4\left(v_p\right) \circ \mathbf{s}_p + \mathcal{N}, \tag{24}$$

where $\mathbf{s}_p = [s_p(t_1), \ldots, s_p(t_K)]^T$ denotes the pth signal, $\mathcal{N} \in \mathbb{C}^{3\times3\times3\times3\times K}$ is the noise tensor, and $\circ$ symbolizes the tensor outer product; see (1) in [4].

As already mentioned, the tensor-ESPRIT requires a shift invariance in each of the N dimensions. For the array in Fig. 7, in the nth mode ($n = 1, \ldots, 4$), the subarray consisting of the first two component-sensors of $\mathbf{a}_r(\cdot)$ and the subarray consisting of the last two component sensors of $\mathbf{a}_r(\cdot)$ are shift invariant. Once the tensor-based signal subspace is obtained, the shift invariance equations for all four modes can be formulated as in (32) of [4]. These shift-invariance equations can be explicitly solved as shown by (34) of [4]. Then, the coarse-but-unambiguous estimates of direction-cosines can be found by solving the shift-invariance equations associated with the first two modes $\mathbf{a}_1(u_p)$ and $\mathbf{a}_2(v_p)$; and the fine-but-cyclically-ambiguous estimates of the direction-cosines can be found by solving the shift-invariance equations associated with the last two modes $\mathbf{a}_3(u_p)$ and $\mathbf{a}_4(v_p)$. To disambiguate the fine estimates, a disambiguation step like the one proposed in [2] is adopted.

For the results presented in this subsection, the first stage of our CP-based algorithm is performed using the Tensorlab toolbox [42]. For the second stage, the minimization of $\mathcal{I}_n$ in (21) is done by the Nelder-Mead simplex algorithm, initialized by the estimates of the previous step $\mathbf{k}^*_{p,n-1}$. Random values, within the parameters' respective support regions, are used to initialize the minimization of $\mathcal{I}_1 = \mathcal{J}_1$.

The considered signal scenario in this subsection involves two equal-power narrowband sources impinging respectively from ($u_1 = 0.83$, $v_1 = 0.17$), and ($u_2 = 0.13$, $v_2 = 0.79$). There are $I = 1000$ independent Monte-Carlo runs for each data point on the figures. The additive white noise is complex-value Gaussian distributed. For a fuller comparison, we added on the plots presented in this sections the results for the dual-size ESPRIT of [2].

The first experiment evaluates the performance of the four considered algorithms for different SNRs, in a statistically independent sources scenario. Figs. 8a and 8b plot the CRMSE for 10 and 50 snapshots, respectively. At low SNRs and for a small number of snapshots, the proposed method performs better than the ESPRIT-based algorithms. As expected, when the SNR and/or the number of snapshots increases (Fig. 8b), all the methods present similar performance.

In the second experiment, we compare our CP method with the other algorithms for a fixed SNR of 6 dB and various numbers of snapshots K. Fig. 9 shows that the proposed algorithm can give better results than tensor-ESPRIT and dual-sized ESPRIT where only a small number of snapshots is available. As the number of snapshots increases, all the considered approaches yield similar results.

In a third experiment, the behavior of the four methods is analyzed with respect to the intergrid spacing Δ, which

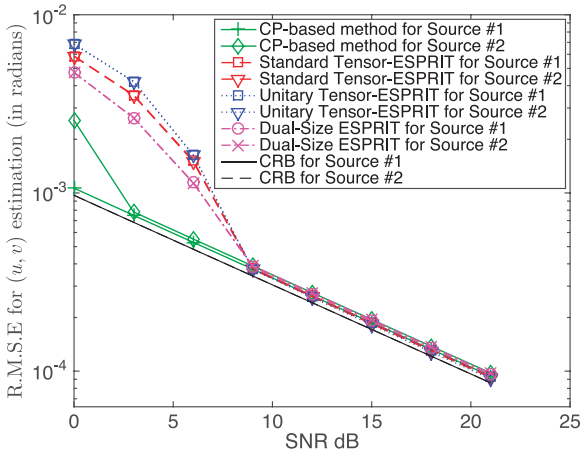

(a) $K = 10$

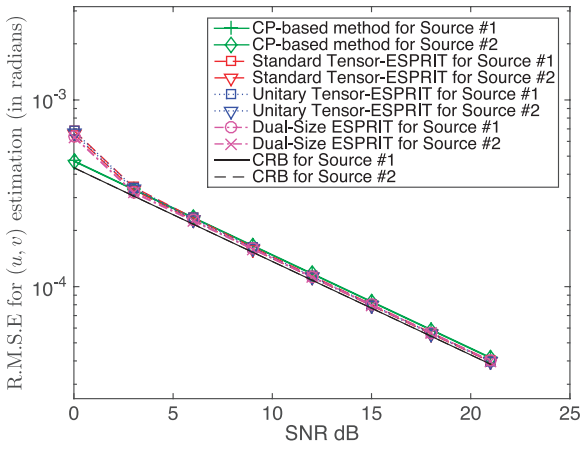

(b) $K = 50$

Fig. 8. Statistically independent sources: CRMSE versus signal-to-noise power ratio (SNR).

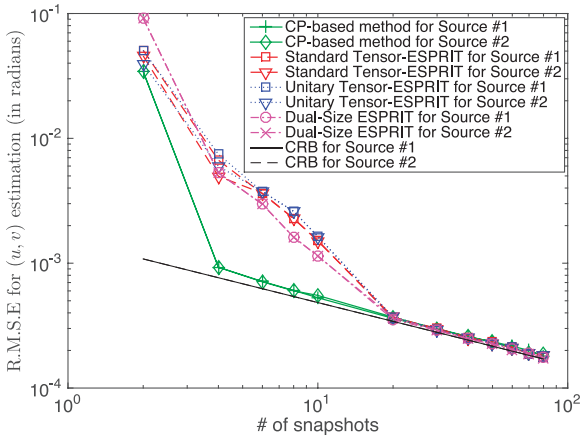

Fig. 9. Statistically independent sources: CRMSE versus number of snapshots when SNR = 6 dB.

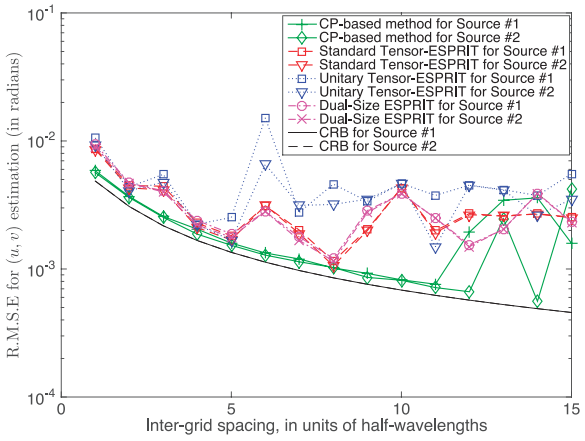

Fig. 10. Statistically independent sources: CRMSE versus intergrid spacing when SNR = 6 dB and number of snapshots $K = 5$.

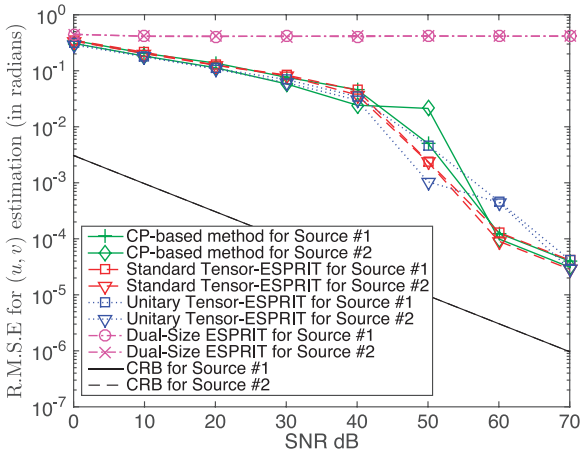

Fig. 11. Statistically independent sources: CRMSE versus signal-to-noise power ratio (SNR) using one temporal snapshot.

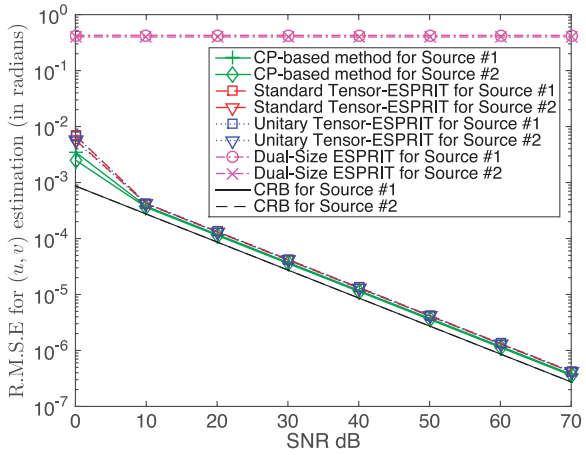

(a) $K = 10, \rho = 1$

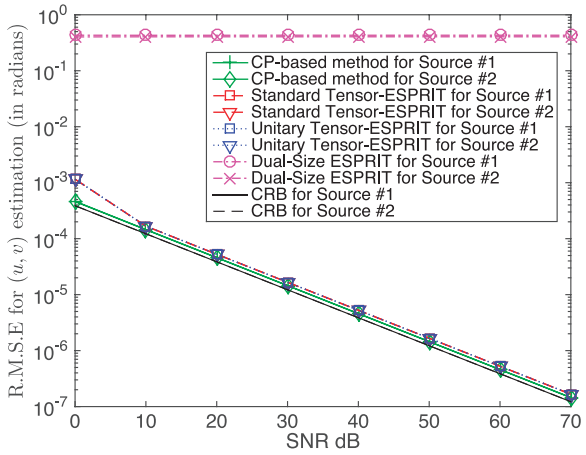

(b) $K = 50, \rho = 1$

Fig. 12. Two cross-correlated sources with correlation coefficient $\rho = 1$: CRMSE versus signal-to-noise power ratio (SNR).

varies within the range [0, 15] $\lambda/2$; the SNR is set to 6 dB; and the number of samples $K = 5$. It can be observed in Fig. 10 that our algorithm (more precisely, the disambiguation stage of our algorithm) is generally more robust to the intergrid spacing than the disambiguation procedure used by the ESPRIT-based methods. However, as Δ increases, all methods fail. This phenomenon can be avoided, for the proposed approach, by gradually increasing the intergrid spacing across the four scale levels, as explained in Section V.

Fig. 11 illustrates the results of the fourth experiment, which evaluates the considered algorithms in the single-snapshot scenario. In this case, prior to using tensor-ESPRIT, a tensor-based spatial smoothing preprocessing step, as developed in Section VI of [4], is applied. It can be observed that our method and the two tensor-ESPRIT algorithms produce similar results, while the approach in [2] fails completely, as expected.

In the last experiment, we compare the proposed approach to the others in the difficult scenario of fully cross-correlated sources. Figs. 12a and 12b plot the results of this experiment, with respect to the SNR for two different number of snapshots $K = 10$ and $K = 50$, respectively. As before, to apply tensor-ESPRIT in this case, a tensor-based spatial smoothing preprocessing, as developed in Section VI of [4], is necessary. The two figures show that, even for cross-correlated sources, our method performs better at low SNR (<10 dB in these simulations) than tensor-ESPRIT. The difference in the estimation accuracy between the CP-based method and tensor-ESPRIT, at low SNR, becomes even more pronounced as the number of available snapshots increases (Fig. 12b). It can also be observed that dual-size ESPRIT is inapplicable in this case.

C. Discussion

We have shown in this section that, on two different array configurations and for diverse scenarios, the proposed approach provides more accurate results than the methods in [2, 3] and the tensor-ESPRIT approach of [4]. For the simulations presented in sub-Section VIA, the gain in the estimation accuracy comes at the expense of a smaller number of sources that can generally be estimated by our method. For a $Q_1 \times Q_2$ grid of five-element half-wavelength spaced cross-shaped subarrays, the

approaches in [2, 3] can handle only up to

$$P \leq \min\{5\,(Q_1-1)\,Q_2-1,\, 5Q_1\,(Q_2-1) -1,\, 2Q_1Q_2-1\} \tag{25}$$

not fully cross-correlates sources, while the number of sources P that can be handled by our approach is given by

$$\min(5,\, P)+\min(Q_1Q_2,\, P)+\min(K,\, P)\geq 2P+2. \tag{26}$$

For the array configuration used in this section, both approaches can handle up to seven sources, but if the size of the grid increases, the number of sources that can be estimated by ESPRIT would increase.

For the array configuration used in sub-Section VIB, in the case of multiple snapshots and not fully cross-correlated sources, a similar analysis shows that our CP-based method can handle up to eight sources; meanwhile, at most $\min\{81, K\}$ sources can be estimated by standard tensor-ESPRIT and at most $\min\{81, 2K\}$ sources by unitary tensor-ESPRIT. This analysis becomes more complicated for tensor-ESPRIT when the spatial smoothing procedure is applied. A drawback of the proposed method is the computational burden, which is generally heavier than for the ESPRIT-based methods. However, powerful CP-fitting algorithms [38, 40] have been developed in recent years, and they significantly improve the convergence speed. Moreover, closed-form solutions exist for CP decompositions [44] that are particularly efficient for Vandermonde-structured data [45, 46], which frequently appears in array processing, and that allow a computational complexity equivalent to ESPRIT's. Nevertheless, for the approaches in [2, 3], two pairing procedures (that may fail for difficult scenarios) are necessary to identify the source parameters. For tensor-ESPRIT, the pairing of the sources across the modes is accomplished by a simultaneous diagonalization algorithm that may exhibit convergence problems. This pairing step is no longer needed with our method because it is implicitly accomplished by the CP decomposition. Compared to tensor-ESPRIT, our algorithm is more flexible because it can be applied to arrays that do not present the shift-invariance feature in each mode, for example, the arrays represented in Figs. 1 and 2.

VII. CONCLUSIONS

This paper introduces a new sensor-array configuration for DOA estimation based on a scale-invariance principle; and we prove that the data acquired by this array follows a multidimensional CP structure. Our analysis proves that this model is identifiable, under only mild conditions that may be met readily in practical applications. A two-stage algorithm for DOA estimation with such an array is proposed and compared with the ESPRIT-based approach developed in [2] and to the ESPRIT-MUSIC algorithm in [3]. Our Monte Carlo simulations verify that our proposed method produces lower mean-square errors than the two earlier ESPRIT-based approaches [2, 3], especially for the case of few snapshots and the case of cross-correlated sources. Moreover, unlike the ESPRIT-based approaches in [2, 3], this proposed algorithm can also be applied to the single-snapshot scenario. Unlike the tensor-ESPRIT approach of [4], our algorithm is not limited to arrays presenting shift invariance in each mode; the numerical simulations show that the proposed method yields more accurate results than tensor-ESPRIT at low SNR and for a small number of samples.

APPENDIX. DERIVATION OF THE FISHER INFORMATION MATRIX FOR THE DATA MODEL IN SECTION VI

The K snapshots, collected by the L-element array using a sampling period T_s can be written as

$$\mathbf{z}=\left[\mathbf{z}(T_s)^T,\cdots,\mathbf{z}(KT_s)^T\right]^T=\sum_{p=1}^{P}\mathbf{s}_p\otimes\mathbf{a}\left(\mathbf{k}_p\right) +\underbrace{\left[\mathbf{n}(T_s)^T,\cdots,\mathbf{n}(KT)_s)^T\right]^T}_{\stackrel{\text{def}}{=}\mathbf{n}}, \tag{27}$$

where $\mathbf{s}_p=[s_p(T_s),\cdots,s_p(KT_s)]^T$, $\otimes$ symbolizes the Kronecker product, and $\mathbf{n}$ represents a $LK\times 1$ noise vector. All unknown but deterministic entities are collected into a $2P\times 1$ vector $\boldsymbol{\psi}=[u_1,\ldots,u_P,v_1,\ldots,v_P]$. The resulting Fisher information matrix $\mathbf{J}$ has its (i,j)th entry equal to (i.e., (8.34) in [47])

$$[\mathbf{J}(\boldsymbol{\psi})]_{i,j}=K\ \mathrm{Tr}\left[\mathbf{R}_{zz}^{-1}\frac{\partial\mathbf{R}_{zz}}{\partial[\boldsymbol{\psi}]_i}\mathbf{R}_{zz}^{-1}\frac{\partial\mathbf{R}_{zz}}{\partial[\boldsymbol{\psi}]_j}\right], \tag{28}$$

where $\mathbf{R}_{zz}$ represents the data spatial covariance matrix and Tr[.] symbolizes the matrix trace operator.

The received data's spatial covariance matrix, at a given time instant kT_s, is given by

$$\mathbf{R}_{zz}\stackrel{\text{def}}{=}E\left\{\mathbf{z}(kT_s)\,\mathbf{z}(kT_s)^H\right\}=\boldsymbol{\Gamma}_{ss}+\boldsymbol{\Gamma}_{nn}, \tag{29}$$

where

$$\boldsymbol{\Gamma}_{ss}\stackrel{\text{def}}{=}E\left\{\left(\sum_{p=1}^{P}s_p(kT_s)\otimes\mathbf{a}_p\left(\mathbf{k}_p\right)\right)\left(\sum_{p=1}^{P}s_p(kT_s)\otimes\mathbf{a}_p\left(\mathbf{k}_p\right)\right)^H\right\}, \tag{30}$$

$$\boldsymbol{\Gamma}_{nn}\stackrel{\text{def}}{=}E\left\{\mathbf{n}(kT_s)\,\mathbf{n}(kT_s)^H\right\}=\sigma_n^2\mathbf{I}_L, \tag{31}$$

respectively denote the sources' and noise's spatial covariance matrices, with the noise's variance represented as σ_n^2 and $\mathbf{I}_L$ symbolizing an $L\times L$ identity matrix. We conclude that:

1) For two zero-mean unit-variance complex-value Gaussian signals that are statistically independent

(Figs. 3–5),

$$\mathbf{\Gamma}_{ss} = \sum_{p=1}^{2} \sigma_p^2 \mathbf{a}_p \mathbf{a}_p^H, \tag{32}$$

with the pth source's variance as σ_p^2.

2) For two cross-correlated zero-mean unit-variance complex-value Gaussian signals with a cross-correlation coefficient ρ (Fig. 6),

$$\mathbf{\Gamma}_{ss} = \rho\sigma_1\sigma_2 \left(\mathbf{a}_1 \mathbf{a}_2^H + \mathbf{a}_2 \mathbf{a}_1^H\right) + \sum_{p=1}^{2} \sigma_p^2 \mathbf{a}_p \mathbf{a}_p^H.$$

REFERENCES

[1] Sidiropoulos, N. D., Bro, R., and Giannakis, G. B.
Parallel factor analysis in sensor array processing.
IEEE Transactions on Signal Processing, **48**, 8 (Aug. 2000), 2377–2388.

[2] Wong, K. T., and Zoltowski, M. D.
Direction-finding with sparse rectangular dual-size spatial invariance arrays.
IEEE Transactions on Aerospace and Electronic Systems, **34**, 4 (Oct. 1998), 1320–1336.

[3] Zoltowski, M. D., and Wong, K. T.
Closed-form eigenstructure-based direction finding using arbitrary but identical subarrays on a sparse uniform cartesian array grid.
IEEE Transactions on Signal Processing, **48**, 8 (Aug. 2000), 2205–2210.

[4] Haardt, M., Roemer, F., and Del Galdo, G.
Higher-order SVD-based subspace estimation to improve the parameter estimation accuracy in multidimensional harmonic retrieval problems.
IEEE Transactions on Signal Processing, **56**, 7 (Jul. 2008), 3198–3213.

[5] Bienvenu, G., and Kopp, L.
Principe de la goniométrie passive adaptative.
In *Proceedings 7°Colloque sur le traitement du signal et des images, GRETSI*, Nice, France, 1979.

[6] Schmidt, R. O.
A signal subspace approach to multiple emitter location and spectral estimation. Ph.D. dissertation, Stanford University, Stanford, CA, 1981.

[7] Roy, R., and Kailath, T.
ESPRIT-estimation of signal parameters via rotational invariance techniques.
IEEE Transactions on Acoustics, Speech, and Signal Processing, **37**, 7 (Jul. 1989), 984–995.

[8] Liang, J., Yang, S., Zhang, J., Gao, L., and Zhao, F.
4D near-field source localization using cumulant.
EURASIP Journal on Advances in Signal Processing, **2007**, 1 (Jan. 2007), 1–10.

[9] Liang, J.
Joint azimuth and elevation direction finding using cumulant.
IEEE Sensors Journal, **9**, 4 (Apr. 2009), 390–398.

[10] Guo, X., Miron, S., and Brie, D.
Three-way array analysis on polarized signals for direction-finding and blind source separation.
In *Proceedings IAR 2007*, Grenoble, France, Nov. 2007.

[11] Zhang, X., and Xu, D.
Deterministic blind beamforming for electromagnetic vector sensor array.
Progress in Electromagnetics Research, **84** (2008), 363–377.

[12] Guo, X., Miron, S., Brie, D., Zhu, S., and Liao, X.
A CANDECOMP/PARAFAC perspective on uniqueness of DOA estimation using a vector sensor array.
IEEE Transactions on Signal Processing, **59**, 7 (Jul. 2011), 3475–3481.

[13] Miron, S., Guo, X., and Brie, D.
DOA estimation for polarized sources on a vector-sensor array by PARAFAC decomposition of the fourth-order covariance tensor.
In *Proceedings 16th EUSIPCO, Lausanne*, Switzerland, Aug. 2008.

[14] Gong, X.
Source localization via trilinear decomposition of cross covariance tensor with vector-sensor arrays.
In *Proceedings 2010 Seventh International Conference on Fuzzy Systems and Knowledge Discovery (FSKD 2010)*, Yantai, Shandong, China, Aug. 2010.

[15] Nion, D., and Sidiropoulos, N.
A PARAFAC-based technique for detection and localization of multiple targets in a MIMO radar system.
In *Proceedings. of IEEE International Conference on Acoustics, Speech, and Signal Processing 2009*, Taipei, Apr. 2009, 2077–2080.

[16] Gong, X.-F., Liu, Z.-W., and Xu, Y.-G.
Regularised parallel factor analysis for the estimation of direction-of-arrival and polarisation with a single electromagnetic vector-sensor.
IET Signal Processing, **5**, 4 (Jul. 2011), 390–396.

[17] Zhang, X., Ben, D., and Chen, C.
Coherent angle estimation in bistatic multi-input multi-output radar using parallel profile with linear dependencies decomposition.
IET Radar Sonar & Navigation, **7**, 8 (Oct. 2013), 867–874.

[18] Miron, S., Le Bihan, N., and Mars, J. I.
Vector sensor MUSIC for polarized seismic sources localization.
EURASIP Journal on Advances in Signal Processing, **2005**, 1 (Jan. 2005), 74–84.

[19] Gong, X., Liu, Z., Xu, Y., and Ahmad, M. I.
Direction-of-arrival estimation via twofold mode-projection.
Signal Processing, **89**, 5 (May 2009), 831–842.

[20] Boizard, M., Ginolhac, G., Pascal, F., Miron, S., and Forster, P.
Numerical performance of a tensor music algorithm based on HOSVD for a mixture of polarized sources.
In *Proceedings 21st European Signal Processing Conference (EUSIPCO 2013)*, Marrakech, Morocco, Sep. 2013.

[21] Lim, L.-H., and Comon, P.
Blind multilinear identification.
IEEE Transactions on Information Theory, **60**, 2 (Feb. 2014), 1260–1280.

[22] Sundaram, K., Mallik, R., and Murthy, U.
Modulo conversion method for estimating the direction of arrival.
IEEE Transactions on Aerospace and Electronic Systems, **36**, 4 (Oct. 2000), 139–1396.

[23] Goodman, N., and Stiles, J.
Resolution and synthetic aperture characterization of sparse radar arrays.
IEEE Transactions on Aerospace and Electronic Systems, **39**, 3 (Jul. 2003), 921–935.

[24] Athley, F., Engdahl, C., and Sunnergren, P.
On radar detection and direction finding using sparse arrays.
IEEE Transactions on Aerospace and Electronic Systems, **43**, 4 (Oct. 2007), 1319–1333.

[25] Liao, B., and Chan, S.-C.
Direction-of-arrival estimation in subarrays-based linear sparse arrays with gain/phase uncertainties.
IEEE Transactions on Aerospace and Electronic Systems, **49**, 4 (Oct. 2013), 2268–2280.

[26] Hu, N., Ye, Z., Xu, X., and Bao, M.
DOA estimation for sparse array via sparse signal reconstruction.
IEEE Transactions on Aerospace and Electronic Systems, **49**, 2 (Apr. 2013), 760–773.

[27] Pal, P., and Vaidyanathan, P. P.
Nested arrays: A novel approach to array processing with enhanced degrees of freedom.
IEEE Transactions on Signal Processing, **58**, 8 (Aug. 2010), 4167–4181.

[28] Harshman, R. A.
Foundations of the PARAFAC procedure: Models and conditions for an 'explanatory' multimodal factor analysis.
UCLA Working Papers in Phonetics, **16** (Dec. 1970), 1–84.

[29] Carroll, J. D., and Chang, J.-J.
Analysis of individual differences in multidimensional scaling via an N-way generalization of "Eckart-Young" decomposition.
Psychometrika, **35**, 3 (Sep. 1970), 283–319.

[30] Kolda, T. G., and Bader, B. W.
Tensor decompositions and applications.
SIAM Review, **51**, 3 (Sep. 2009), 455–500.

[31] Bro, R., Harshman, R. A., Sidiropoulos, N. D., and Lundy, M. E.
Modeling multi-way data with linearly dependent loadings.
Journal of Chemometrics, **23**, 7–8 (Jul.-Aug. 2009), 324–340.

[32] Swindlehurst, A. L., Ottersten, B., Roy, R., and Kailath, T.
Multiple invariance ESPRIT.
IEEE Transactions on Signal Processing, **40**, 4 (Apr. 1992), 867–881.

[33] Kruskal, J. B.
Three-way arrays: Rank and uniqueness of trilinear decompositions, with application to arithmetic complexity and statistics.
Linear Algebra and Its Applications, **18**, 2 (1977), 95–138.

[34] Sidiropoulos, N. D., and Bro, R.
On the uniqueness of multilinear decomposition of N-way arrays.
Journal of Chemometrics, **14**, 3 (2000), 229–239.

[35] Guo, X., Miron, S., Brie, D., and Stegeman, A.
Uni-mode and partial uniqueness conditions for CANDECOMP/PARAFAC of three-way arrays with linearly dependent loadings.
SIAM Journal on Matrix Analysis and Applications, **33**, 1 (2012), 111–129.

[36] Zhang, L., Huang, T.-Z., Zhu, Q.-F., and Feng, L.
Uni-mode uniqueness conditions for CANDECOMP/PARAFAC decomposition of n-way arrays with linearly dependent loadings.
Linear Algebra and Its Applications, **439**, 7 (Oct. 2013), 1918–1928.

[37] Bro, R., and Andersson, C. A.
Improving the speed of multiway algorithms. Part II: Compression.
Chemometrics and Intelligent Laboratory Systems, **42**, 1–2 (1998), 105–113.

[38] Bro, R., Sidiropoulos, N. D., and Giannakis, G. B.
A fast least squares algorithm for separating trilinear mixtures.
In *Proceedings of the International Workshop Independent Component Analysis and Blind Signal Separation (ICA'99)*, Aussois, France, Jan. 1999.

[39] Rajih, M., Comon, P., and Harshman, R. A.
Enhanced line search: A novel method to accelerate PARAFAC.
SIAM Journal on Matrix Analysis and Applications, **30**, 3 (Jan. 2008), 1128–1147.

[40] Tomasi, G., and Bro, R.
A comparison of algorithms for fitting the PARAFAC model.
Computational Statistics & Data Analysis, **50** (2006), 1700–1734.

[41] Andersson, C. A., and Bro, R.
The N-way toolbox for MATLAB.
Chemometrics and Intelligent Laboratory Systems, **52** (2000), 1–4.

[42] Sorber, L., Van Barel, M., and De Lathauwer, L.
Tensorlab v1.0.
Available: http://esat.kuleuven.be/sista/tensorlab/. Accessed Feb. 2013.

[43] Blake, A., and Zisserman, A.
Visual Reconstruction (*Artificial Intelligence Series*).
Cambridge, MA: MIT Press, 1987.

[44] Roemer, F., and Haardt, M.
A closed-form solution for parallel factor (PARAFAC) analysis.
in *Proceedings of ICASSP*, Las Vegas, NV, Mar. 2008, 2365–2368.

[45] Sorensen, M., and De Lathauwer, L.
Tensor decompositions with Vandermonde factor and applications in signal processing.
In *Proceedings of the Asilomar Conference on Signals, Systems and Computers*, Pacific Grove, CA, Nov. 2012.

[46] Sorensen, M., and De Lathauwer, L.,
Blind signal separation via tensor decomposition with Vandermonde factor: Canonical polyadic decomposition.
IEEE Transactions on Signal Processing, **61**, 22 (Nov. 2013), 5507–5519.

[47] Van Trees, H. L. Detection, Estimation, and Modulation Theory, Part IV: Optimum Array Processing. New York, NY: John Wiley & Sons, Inc., 2002.

Sebastian Miron graduated from Technical University of Iasi, Romania, in 2001 and received the M.Sc. and Ph.D. degrees in signal, image, and speech processing from the Institut National Polytechnique of Grenoble, France, in 2002 and 2005, respectively. He is currently a maître de conférence (associate professor) at Université de Lorraine, France, and he is conducting research at the Centre de Recherche en Automatique de Nancy (CRAN), Nancy, France.

He was conferred the *Best Ph.D. Award* by the Institut National Polytechnique of Grenoble in 2005. He is on the editorial board of *Physical Communication* journal since 2012. His current research interests include vector-sensor-array processing, spectroscopy and microscopy data processing, positive source separation, multidimensional signal processing, and multilinear algebra.

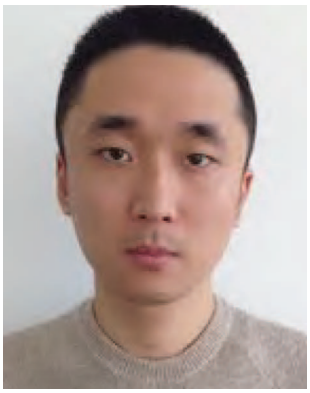

Yang Song obtained his B. Eng. degree in Communication Engineering in 2007 from Zhejiang University City College, Hangzhou, Zhejiang, China. He received an M.Eng. in 2008 and a Ph.D. in 2013, both in electronic and information engineering, from the Hong Kong Polytechnic University, where he was a Research Associate until January 2014. Thereafter, he has been a visiting researcher at Universität Paderborn, Paderborn, North Rhine-Westphalia, Germany. His research interest relates to space-time signal processing.

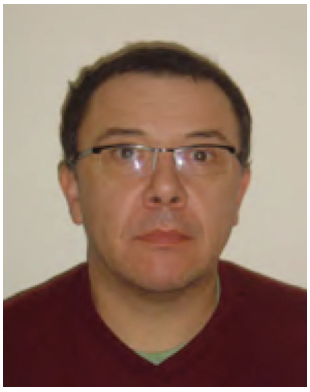

David Brie received the Ph.D. degree in 1992 and the *Habilitation à Diriger des Recherches* degree in 2000, both from the Henri Poincaré University, Nancy, France. He is currently full professor at the Department of Telecommunications and Networking of the Institut Universitaire de Technologie, Université de Lorraine, France.

He is editor-in-chief of the *Traitement du Signal* journal since 2013. Since 1990, he has been with the Centre de Recherche en Automatique de Nancy, France. His research interests mainly concern inverse problems and multidimensional signal processing.

Kainam Thomas Wong (SM'01), earned the B.S.E. degree in chemical engineering from the University of California, Los Angeles, California, in 1985, the B.S.E.E. degree from the University of Colorado, Boulder, Colorado, in 1987, the M.S.E.E. degree from the Michigan State University, East Lansing, Michigan, in 1990, and a Ph.D. degree in electrical and computer engineering from Purdue University, West Lafayette, Indiana, in 1996.

He was a manufacturing engineer at the General Motors Technical Center, Warren, Michigan, from 1990 to 1991, and a senior professional staff member at the Johns Hopkins University Applied Physics Laboratory, Laurel, Maryland, from 1996 to 1998. He was a regular member of the faculty at Nanyang Technological University, Singapore, in 1998, the Chinese University of Hong Kong in 1998–2001, and the University of Waterloo, Waterloo, Ontario, Canada, in 2001–2006. Since 2006, he has been with The Hong Kong Polytechnic University as an associate professor.

He was on the editorial boards of *Circuits, Systems, and Signal Processing* in 2007–2009, the *IEEE Signal Processing Letters* in 2006–2010, the *IEEE Transactions on Aerospace and Electronic Systems* since 2012, the *IEEE Transactions on Signal Processing* in 2008–2012, the *IEEE Transactions on Vehicular Technology* in 2007–2013, *Physical Communication* in 2012–2014, *IET Microwaves, Antennas & Propagation* since 2014, and *IET Radar, Sonar & Navigation* since 2015. He is an elected member of the IEEE Signal Processing Society's technical committee on sensor and multichannel processing (SAM), for 2013–2015. His research interest includes sensor-array signal processing and signal processing for communications. He was conferred the *Premier's Research Excellence Award* by the Canadian province of Ontario in 2003.